

Hydrogen embrittlement of Zn-, Zn–Ni-, and Cd-coated high strength steel

K. R. Sriraman · S. Brahimī · J. A. Szpunar · S. Yue

Received: 7 November 2012 / Accepted: 9 January 2013 / Published online: 20 January 2013
© Springer Science+Business Media Dordrecht 2013

Abstract Sacrificial coatings, such as Zn and Cd, are used to protect steel against corrosion. During the electrodeposition of metals, hydrogen is evolved due to electrolysis. The evolved hydrogen may diffuse outward and become trapped in the substrate/coating interface or migrate inward into the steel lattice causing delayed embrittlement when the component is subjected to stress. This study reports two principal variables for Zn, Zn–Ni, and Cd coatings: (i) the quantity of hydrogen absorbed by the coating and substrate by vacuum thermal desorption and (ii) the permeability of the coating material to hydrogen by electrochemical permeation. The findings were analyzed in correlation with the microstructural characteristics of both the coating material and the coating/substrate interface. With Zn–Ni, both coating process and coating material combined to significantly reduce the risk of internal hydrogen embrittlement by (i) introducing the least amount of hydrogen during the electrodeposition process and (ii) by the ease with which hydrogen can be extracted by baking due to the presence of cracks in the coating.

Keywords Electrodeposited Zn–Ni · Cd · Zn coatings · Thermal desorption · H₂ permeability

K. R. Sriraman (✉) · S. Brahimī · S. Yue
Department of Mining & Materials Engineering,
McGill University, Montreal, QC, Canada
e-mail: sriraman.rajagoapalan@mail.mcgill.ca

S. Brahimī
IBECA Technologies Corp, Montreal, QC, Canada

J. A. Szpunar
Department of Mechanical Engineering,
University of Saskatchewan, Saskatoon, SK, Canada

1 Introduction

Hydrogen embrittlement is an infrequent yet insidious problem that can lead to sudden catastrophic failure of high strength steel components. Hydrogen is practically insoluble in steel at room temperature. It can either remain trapped in microstructural features such as defects and inclusions or it can become mobile within the steel matrix. Broadly speaking, hydrogen embrittlement is caused by mobile (diffusible) hydrogen. Two primary ingredients present in sufficient quantities will cause hydrogen embrittlement failure of a high strength steel component. These are (i) a critical level of diffusible hydrogen in the microstructure and (ii) a threshold stress that is exceeded by applied stress, residual stress, or a combination of both. Threshold stress is a function of susceptibility of the steel, which is primarily increased with increasing strength, but can also be affected by microstructure. The source of hydrogen can either be external such as with service corrosion, classified under environmental hydrogen embrittlement (EHE), or a result of processing such as steel making, electrodeposition of coatings, or pickling, classified under internal hydrogen embrittlement (IHE) [1, 2]. Hydrogen embrittlement in steel is typically characterized mechanically by various types of slow strain rate tests that quantify the loss of strength and ductility resulting from the migration of diffusible hydrogen to the point of maximum stress concentration. Quantification of hydrogen, notably hydrogen present in bulk metal, is an additional tool for understanding the mechanisms affecting embrittlement of coated high strength steel.

Zn-14 % Ni coatings applied over high strength steel are of interest because they have been shown to have a low propensity for IHE and are also more responsive to baking for hydrogen removal [3]. Zn-14 % Ni coatings also

provide excellent corrosion resistance, comparable to that of pure electrodeposited Cd.

However, the microstructure of Zn–Ni coatings poses a number of contradictory challenges. Coleman et al. [4] investigated the hydrogen permeability of electrodeposited Zn–Ni, Zn, and Ni membranes and found that the permeability of Zn–Ni alloy was comparable to the permeability of both Zn and Ni, which is roughly 80 % lower than that of bare iron. In other words, Zn–Ni is relatively impermeable to hydrogen diffusion. However, other Zn–Ni coatings typically exhibit defects, such as intergranular cracks and through thickness pores, which are formed in the coating by residual stresses in the coating/substrate interface [5]. It has been postulated that these defects may make Zn–Ni coatings susceptible to EHE as they provide pathways for hydrogen diffusion inward from the surface of the coating to the steel substrate [5]. On the other hand, it can also be argued that such defects can facilitate hydrogen diffusion outward from the substrate to the environment.

Other studies performed with Zn-10 % Ni and Zn-1 % Co attributed the lower propensity to IHE than with the pure Zn to the formation of nickel- or cobalt-rich layers in the initial stages of deposition. These layers exhibited even lower hydrogen diffusivity in comparison to Zn, thus acting as barriers to hydrogen absorption during electroplating [6]. An attempt was made to measure the rate of hydrogen absorbed during different plating processes (Zn, Zn–Ni, and Zn–Co) by means of the electrochemical permeation method. The investigators reported that the Zn–Ni plating process exhibited the lowest hydrogen absorption [7].

Another consideration in the elimination of the risk of IHE in high strength steels is the effect of a post-electroplating heat treatment (baking) for eliminating hydrogen. Baking is a standard practice where electroplating of high strength steel is performed. Most notably, the fastener and the aerospace industry standards require electroplated parts to be baked between 4 and 24 h, typically at temperatures not exceeding 200 °C [8]. Hiller and Robinson reported the full recovery of mechanical strength and ductility of electrodeposited Zn, Zn–Ni, Zn–Co, and Cd plated high strength steel specimens [6] after the baking cycle. More specifically, they reported an 89 % recovery for Zn and Zn–Co and 100 % recovery for cadmium and Zn–Ni electroplated specimens after 24 h of baking at 200 °C. This study did not quantify the amount of diffusible hydrogen eliminated during the baking cycles. Additionally, apart from mechanical strength, other aspects such as microstructure, coating permeability, and process generated hydrogen were not addressed.

The current investigation reports two principle parameters: (i) the amount of hydrogen generated due to the plating process of Zn, Zn–Ni, and Cd coatings and (ii) the

hydrogen permeability of the coated steel. These parameters are then correlated with the microstructure of the coating/substrate interface of the coated steel.

2 Experimental methodology

2.1 Substrate materials

Two different types of substrates were utilized in this study: (i) shim stock, 100 µm thick, made of low carbon SAE 1006 steel for coatings that were used for permeation measurements and (ii) ASTM F519 Type 1e specimens which were coated for vacuum thermal desorption experiments [9]. The specimens were notched square bars made of SAE 4340 steel, heat treated to 51–53 Rockwell C. The dimensions of the notch bars are 55.9 mm length, 10 mm width, and 10 mm height.

2.2 Coating processes

The sample substrates (notch bars and shim stock) were coated by the electrodeposition of Zn, Zn–Ni, and Cd using industrial electroplating processes. The basic parameters for the coating processes are listed below. The thicknesses of all the coatings were maintained in the range of 15–20 µm.

2.2.1 Zn–Ni

A commercially available Zn–Ni plating solution IZ C17+ provided by Dipsol Inc. was used. An alkaline plating solution with Zn and Ni metal concentrations in the ratio of 10–11:1 was used. The individual bath constituents were Zn concentrate (9–11 g l⁻¹), Ni concentrate (08–1.2 g l⁻¹), Na₂CO₃ (59 g l⁻¹), and NaOH (135 g l⁻¹). The plating bath efficiency was close to 70 %. The substrates were subjected to various pretreatments like aqueous degreasing, water rinsing, abrasive grit blasting, and acid activation and were plated in an industrial pilot plating tank. The pH of the plating bath was maintained at 12–13.5 at 25 °C and a plating current density of 28–30 mA cm⁻² was applied to produce a coating thickness of 15–20 µm in one hour.

2.2.2 Zn

The plating bath was acid chloride based with ZnCl₂ (60 g l⁻¹), KCl (250 g l⁻¹), H₃BO₃ (25 g l⁻¹), and HCl in smaller concentrations to maintain the pH of the bath to 4.5–4.8. The cathode efficiency was 95 % and the temperature of the plating was held at 25 °C. The electroplating was performed on a laboratory-scale plating setup. A plating current density of 5 mA cm⁻² was used to

generate a coating thickness of 15 μm in 2 h. The substrates were mechanically finished with 600 grit SiC grinding paper and activated in HCl for 10–12 s before plating.

2.2.2.1 Low hydrogen embrittling Cd plating (LHE Cd)
LHE Cd was plated in an industrial plating facility using an alkaline cyanide-based plating solution with CdO (20–30 g l^{-1}), NaCN (90–135 g l^{-1}), Na_2CO_3 (0–60 g l^{-1}), and NaOH (11–30 g l^{-1}) and a plating bath efficiency of close to 70 %. A plating current density of 118–120 mA cm^{-2} was used to generate a coating thickness of 15 μm in 5 min. Substrates were solvent degreased, grit blasted, and acid pickled before plating. The plating temperature was 15–30 $^\circ\text{C}$ [10].

2.3 Characterization of coatings

The coatings were characterized based on surface and interface morphology, thickness determination, and defect distribution with a Philips Field Emission Gun scanning electron microscope (FEG-XL30). The phase distribution, crystal structure, and coatings were determined using a Bruker Discover D8–2D VANTEC 2000 X-ray diffractometer (XRD) with Cu $K\alpha$ source.

2.4 Vacuum thermal desorption spectroscopy

Thermal desorption spectroscopy (TDS) is a versatile method to quantify hydrogen in bulk metals. The method is based on the fact that hydrogen, either in a metal lattice or trapped in various trap sites like dislocations, grain boundaries, diffuses upon heating [11]. Given enough time and energy, hydrogen diffuses outward from the bulk material (desorption) into the atmosphere and can be detected within a closed vacuum system by an analytical instrument, namely a pressure gauge, a gas chromatograph, or a mass spectrometer [12]. The thermal desorption method has been used in previous investigations to determine the amount of hydrogen desorbed from electroplated Zn- and Cr-based coatings [12]. In this investigation, a mass spectrometer was used to measure the quantity of hydrogen being desorbed over time. The TDS schematic is shown in Fig. 1. The specimen chamber is made from ultrahigh vacuum (UHV) grade 304 stainless steel. The chamber is evacuated by means of two turbo molecular pumps backed by two rotary vane pumps. The specimen chamber was used to house the notch bars (bare and coated). The chamber was sealed and then pumped down to a vacuum of less than 5×10^{-6} torr. After achieving the required vacuum, the mass spectrometer was turned on to measure the hydrogen ion intensity. The chamber was heated with a resistive heating tape, and temperature was controlled by means of a temperature

controller connected to a thermocouple that was placed directly on the specimen surface. This mechanism provided direct control and monitoring of the specimen temperature. After the background subtraction, the net hydrogen ion intensity measured by the quadrupole mass spectrometer represented hydrogen being desorbed from the specimen.

2.5 Electrochemical permeation studies on the coated steel

The electrochemical permeation cell schematic is shown in Fig. 2. Bare and coated shim steel sheets were cut to 40 mm \times 40 mm dimensions and finished to 600 grit finish. The twin compartment permeation cell was made of Teflon, with a specimen exposure area of 0.720 cm^{-2} . The cell was placed inside a Faraday cage to minimize external noise or disturbance. A 6 V battery with variable rheostat was used as the charging source. Palladium was sputtered on the steel using a plasma sputtering apparatus. The specimen arrangement was such that the Zn/Cd coating was used as the charging side and the palladium sputtered steel surface was used as the discharge side. The specimen acts as the working electrode for both cells. Platinum wire was used as a counter electrode in both cells. The electrolyte used in the charging side was a mixture of 0.5 M H_3BO_3 and 0.5 M Na_2SO_4 ; As_2O_3 (200 ppm) was added on the charging side as atomic hydrogen recombination poison. A constant current of 0.1 mA was applied to the charging side. The electrolyte used in the discharge side was 0.1 M NaOH. The exit side of the permeation cell was maintained at a constant potential of -300 mV with respect to a standard calomel electrode [13, 14]. After a sufficient time interval, the oxidation current in the anodic side reached less than 50 nA,

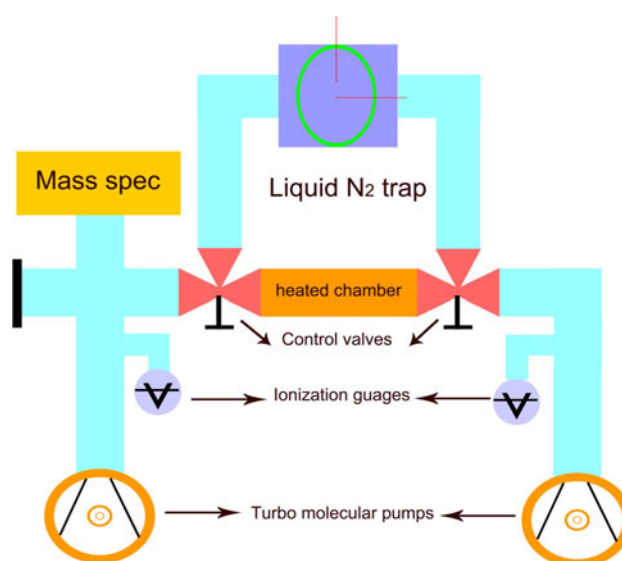


Fig. 1 Vacuum thermal desorption experimental setup

and the hydrogen charging in the cathodic cell was commenced. Hydrogen oxidation current was monitored on the exit side (anodic side) of the permeation cell. This oxidation current was monitored with respect to time and the output was recorded for calculation of diffusion coefficient and the permeation flux. A detailed description of the experimental methodology is given in the literature [13, 14].

3 Results

3.1 Coating characterization

The X-ray diffraction patterns and surface morphologies of the investigated coatings are shown in Figs. 3 and 4, respectively. From Fig. 4, it can be observed that Zn–Ni was composed of large platelets [15] (about 10 μm in size) with intermittent porosity and microcracks. The X-ray diffraction results showed that the Zn–Ni coating was composed of uniform γ -Zn–Ni ($\text{Ni}_2\text{Zn}_{11}$) which is the typical phase observed in Zn–15 % Ni [16–18]. The Zn coating was composed of hemispherical clusters which are typical of most Zn coatings [15, 19]. The Cd coating was composed of

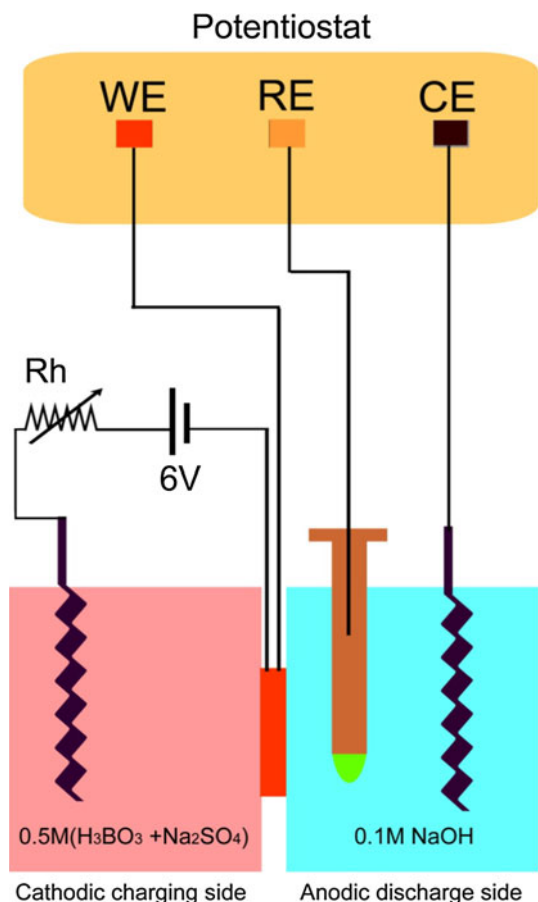


Fig. 2 Electrochemical permeation cell schematic

spherical hexagonal platelets (Fig. 4c). More precisely, these platelets are hexagonal crystals clustered together to form a spherical structure, a common characteristic of Cd coatings [20, 21]. The XRD patterns of Zn and Cd reflected pure metal without any detectable contaminants. The cross-sectional morphologies of the coatings plated on the notch bar are shown in Fig. 5. The Zn–Ni coating consisted of through thickness microcracks which expanded during the heat treatment as shown in Fig. 5. The reason behind the cracks is the inherent lattice strain associated with the formation of γ -Zn–Ni ($\text{Ni}_2\text{Zn}_{11}$). These cracks expanded due to the mismatch in the coefficient of thermal expansion between the substrate and the coating material, accompanied by an increase in the magnitude of residual stress distribution across the coating thickness [22, 23]. The Zn coating had a uniform interface, while the LHE Cd coating had intermittent discontinuities designed to facilitate the removal of co-evolved hydrogen [10].

3.2 Vacuum thermal desorption spectroscopy

The hydrogen discharge distribution of the bare and coated notch bar specimens is shown in Fig. 6. The quadruple mass spectrometer has two types of detectors, namely a Faraday cup and a secondary electron multiplier. In our present investigation, the Faraday cup detector was used. The experimental output of the Faraday cup was hydrogen ion intensity vs. time. The number of hydrogen ions discharged was calculated using Faraday's law:

$$N = \frac{It}{e}$$

N = number of hydrogen ions, I = ion current in amperes, t = time in seconds, and e = charge of an electron

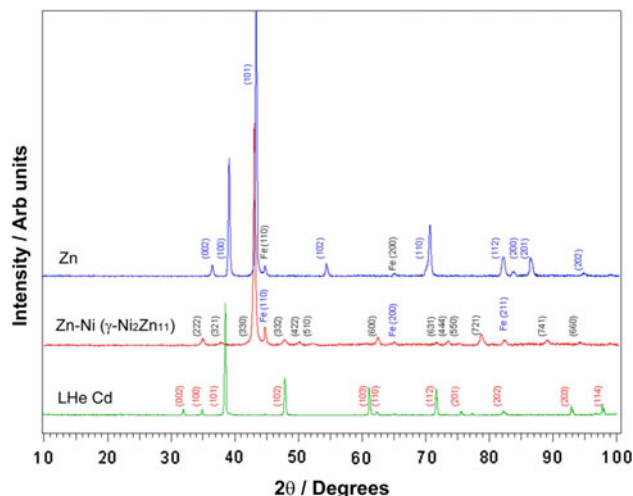


Fig. 3 XRD of the investigated coatings

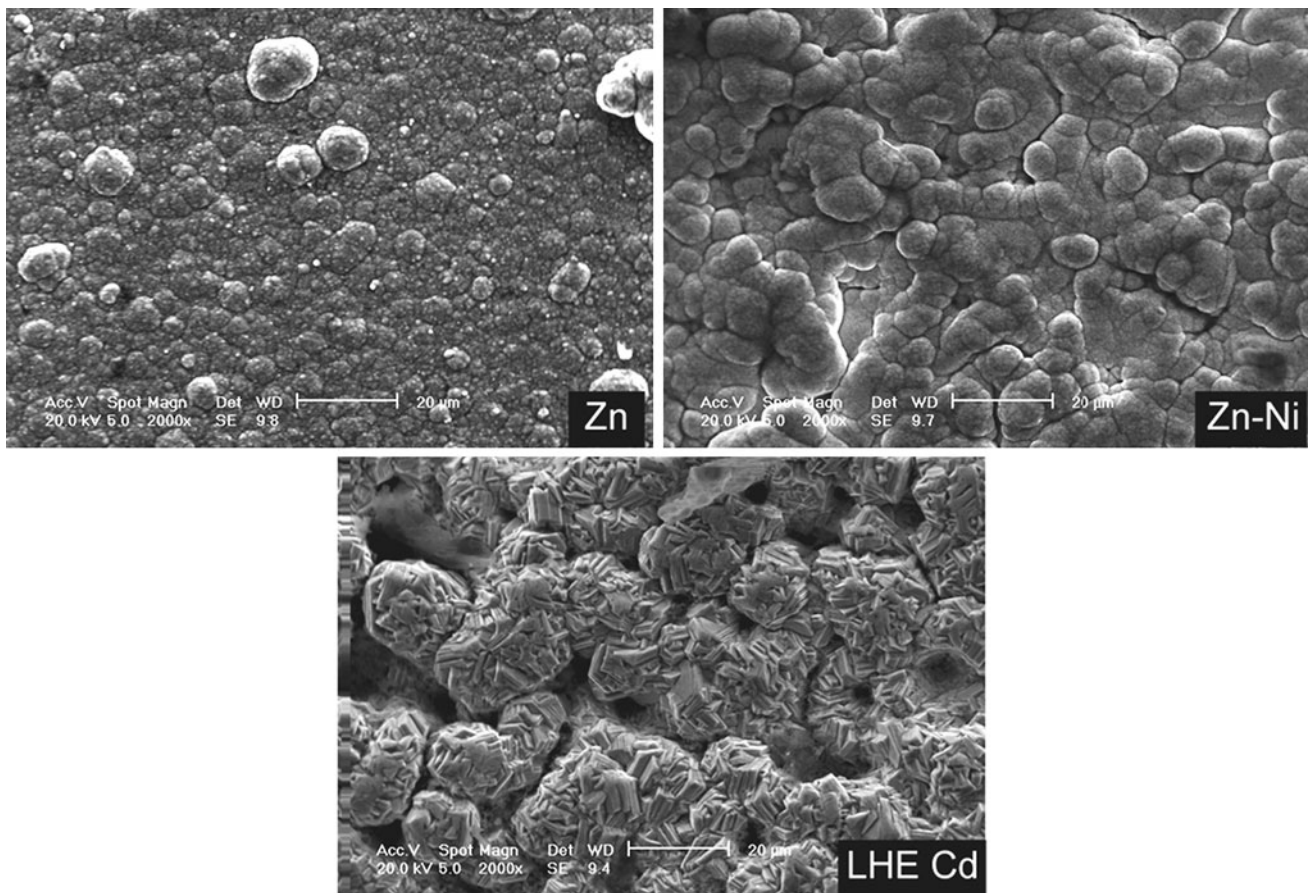


Fig. 4 SEM images of the coating surfaces

1.602×10^{-19} C. The ion count was subsequently converted into parts per million by mass ratio calculations.

From Fig. 6a, in the steel specimen, as baking temperature was varied from 100 to 300 °C, the higher baking temperature resulted in a higher hydrogen discharge. Zn coatings discharged the greatest amount of hydrogen (Fig. 6b) when baked at 300 °C. However, the extreme vacuum also caused the Zn to volatilize at 300 °C. A similar trend was observed for Cd coatings (Fig. 6c) where at 200 °C, Cd was also volatilized. These results indicate that the maximum baking temperatures in this experimental setup were constrained to 200 °C for Zn and 100 °C for Cd for studying the amount of hydrogen discharged from coated specimens.

The results of the TDS studies are summarized in Fig. 7. At 200 °C baking temperature, hydrogen discharge was the lowest for Zn–Ni (0.05×10^{-6} ppm) as compared to Zn (4.41×10^{-6} ppm) and Cd (0.57×10^{-6} ppm). The hydrogen discharged by the coated specimens is attributed to the amount of hydrogen absorbed during the plating process and the permeability of the coating. More precisely, the amount of hydrogen absorbed during the plating process is a function of processing parameters, such as current density,

plating time, batch efficiency, etc., and the permeability of the coating, which is a function of its microstructure and general morphology. If the coating happens to be extremely permeable to hydrogen, as is the case with phosphate coatings [3], it does not act as a barrier to hydrogen diffusion and given sufficient time, hydrogen will escape at room temperature. Defects in the coatings also contribute to hydrogen escape from the matrix. In the case of the Zn coating, as shown in Fig. 5a, the cross section is uniform without any defects, which led to the trapping of hydrogen in the interface, which was then released during the baking process. In the case of the Cd coating, as shown in Fig. 5b, the more discontinuous interface led to the escape of hydrogen from the interface within a short duration of the plating, which was indicated by a lower amount of hydrogen present in the coating. Zn–Ni coatings had inherent microcracks across the interface, Fig. 5c, which expanded during the heat treatment, Fig. 5d, acting as hydrogen escape pathways.

The results appear to indicate that the Zn–Ni process introduced the least amount of hydrogen into the specimens, as compared to Zn and Cd processes.

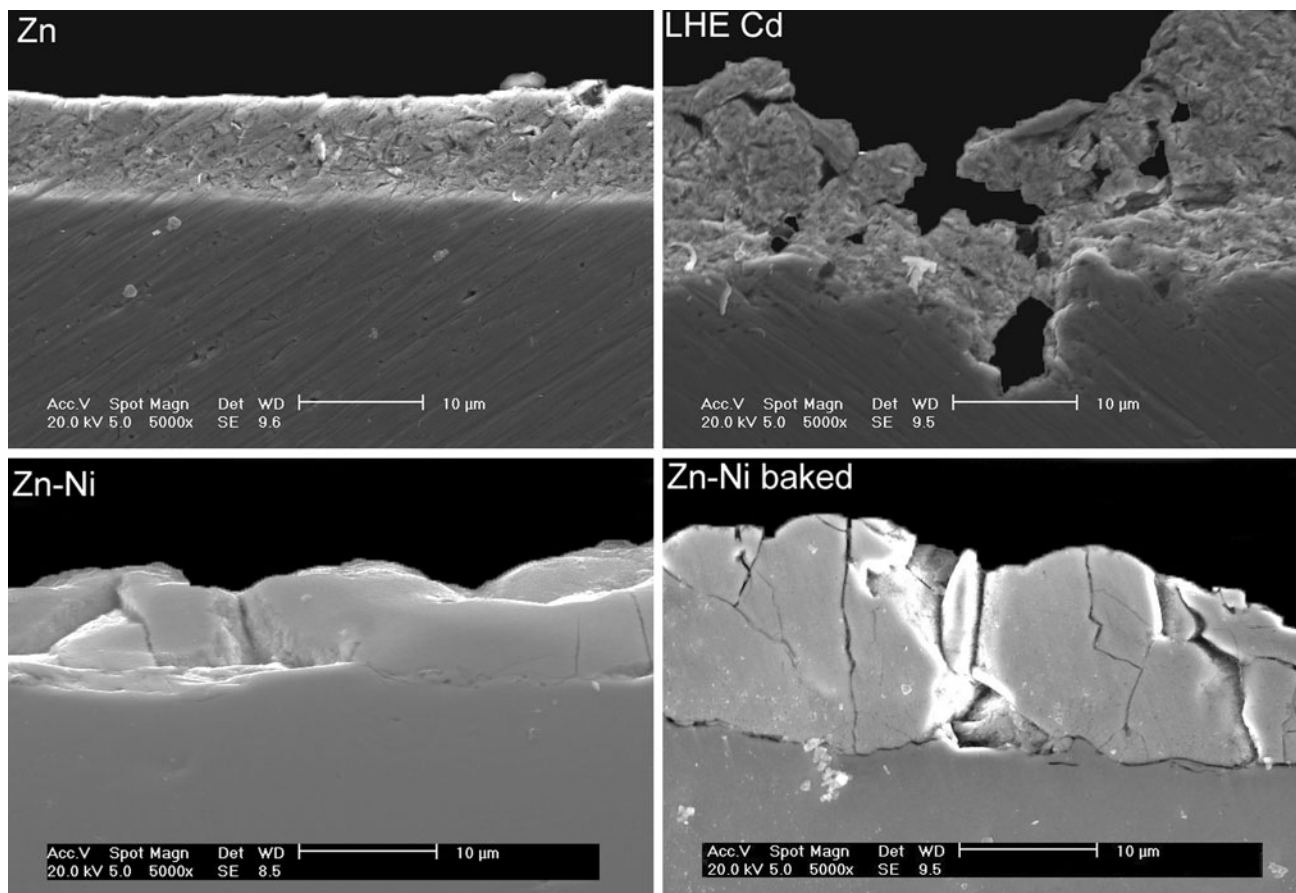


Fig. 5 Cross-sectional SEM images of the investigated coatings on the notch *bar* specimen

3.3 Electrochemical hydrogen permeability of coated steel

The permeability of the steel and coated steel specimens to hydrogen was determined by the twin cell method. A relatively permeable low carbon steel substrate was chosen for the experiments. From the coating cross-sectional morphologies on the notch bar (Fig 5), it was evident that the Zn coating had a uniform defect-free cross section, the Zn–Ni coatings had microcracks, and the Cd coating had intermittent discontinuities. Since the substrate geometry was changed, the microcracks' distribution in the Zn–Ni coatings also changed. The microcracks were randomly distributed with some areas having a uniform cross section as shown in Fig. 8a and a discontinuous cracked microstructure as shown in Fig. 8b. When the low carbon steel shims were subjected to heat treatment at 200 °C, the crack network increased to form a morphology shown in Fig 8c. Similar observations were recorded for the Cd coatings with some areas of the coated shim having a uniform interface as shown in Fig. 9a and with intermittent discontinuities as shown in Fig. 9b. The permeation tests were performed on both uniform and non-uniform coating

interfaces. The output of the experiments is permeation current density versus time as shown in Fig. 10. Figure 10a shows the current transient characteristics of the bare SAE 1006 steel and Fig. 10b shows the transient behaviors of uniform defect-free Zn, Zn–Ni, and Cd coatings on steel substrate. From the current transient graphs, the diffusion coefficient, the subsurface hydrogen concentration, and the steady state permeation flux were determined using the following equations [24–26]:

$$D_{\text{eff}} = \frac{L^2}{2 * t_{\text{lag}}} \quad D_{\text{eff}} = \frac{L^2}{12.98 * t_b} \quad J_{\text{SS}} = \frac{I_{\text{SS}}}{A * F} \quad (1)$$

$$C_0 = \frac{J_{\text{SS}}}{L * D_{\text{eff}}}$$

D_{eff} = effective diffusion coefficient ($\text{cm}^2 \text{s}^{-1}$); J_{SS} = steady state permeation flux ($\text{mol s}^{-1} \text{cm}^{-2}$); C_0 = subsurface hydrogen ion concentration (mol cm^{-3}); I_{SS} = steady state permeation current (A); T_b = breakthrough time (s); and t_{lag} = time lag— $0.63 t_{\text{ss}}$, t_{ss} = steady state time (s); L = Membrane thickness; and A = exposed area (cm^{-2}).

From Fig. 10a, it can be observed that SAE 1006 steel was easily permeable to atomic hydrogen, which was evident from a very short breakthrough time (10 s) and a

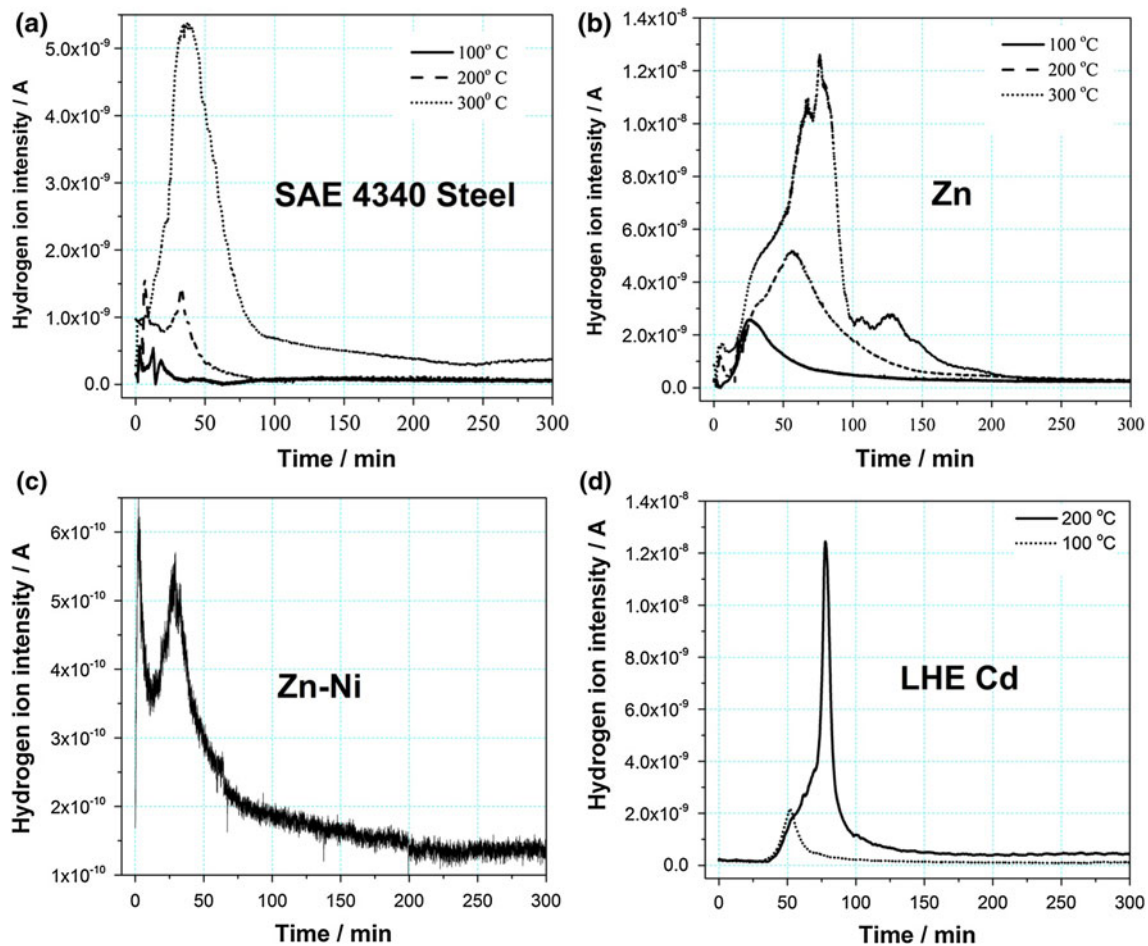


Fig. 6 TDS ion intensity spectrum for **a** substrate steel, **b** Zn, **c** Zn–Ni, **d** LHE Cd from the mass spectrometer

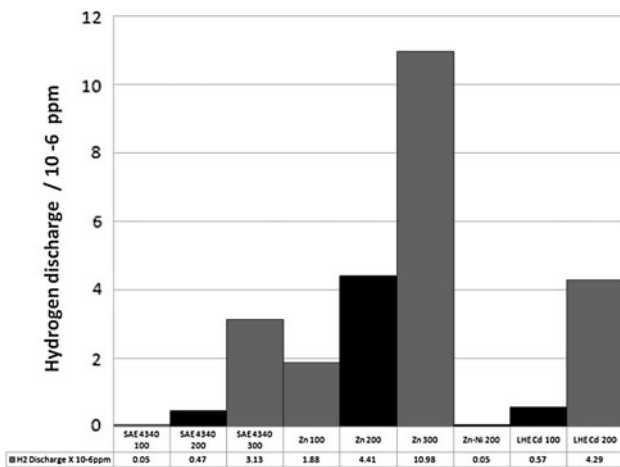


Fig. 7 Summary of TDS data of the substrate and coatings at different temperature

very high permeation current density ($8.52 \mu\text{A cm}^{-2}$). Figure 10b shows the permeation characteristic of Zn-, Zn–Ni-, and Cd-coated steel surfaces. From Fig. 10b, it is evident that all the three coatings, Zn, Zn–Ni, and Cd,

acted as a barrier for hydrogen diffusion in steel. This is evident by the fact that the permeation current density was drastically reduced and the breakthrough time was increased significantly, 720 s for Zn, 6,400 s for Zn–Ni, and 365 s for Cd, as compared to the 10 s for steel substrate alone. Using Eq. (1) mentioned above, the diffusion coefficients were calculated for the coated steels, which are listed in Table 1. The effective diffusion coefficients and the steady state hydrogen permeation flux of Zn–Ni coatings were one order of magnitude lower compared to the Zn- and Cd-coated steel, which indicated that Zn–Ni coatings offer much better barriers to hydrogen diffusion than Zn and Cd coatings.

Figure 11a shows the H_2 permeation transient of Zn–Ni-coated steel with microcracks and Fig. 11b shows the transient of Cd-coated steel with discontinuities. It can be observed that the breakthrough time was a lot shorter, 140 s as opposed to 6,400 s in the case of Zn–Ni and 25 s as opposed to 350 s in the case of Cd coatings. Steady state permeation flux was higher in both the cases than the steel with a uniform coating interface. The hydrogen permeation

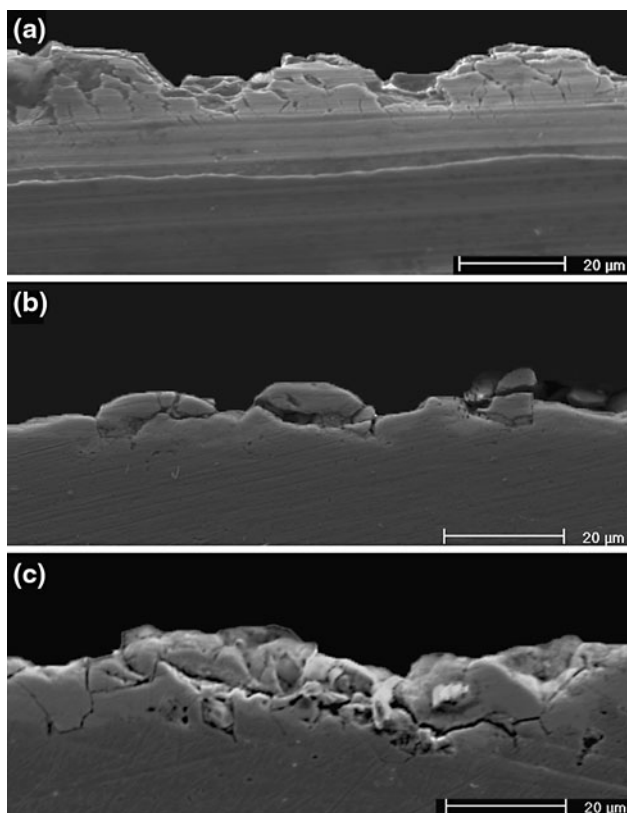


Fig. 8 Cross-sectional SEM images of Zn–Ni coatings on low carbon steel shims **a** uniform defect-free cross section, **b** as-plated Zn–Ni coatings with discontinuities and microcracks, **c** Zn–Ni cross section after post-baking heat treatment with microcracks and discontinuities

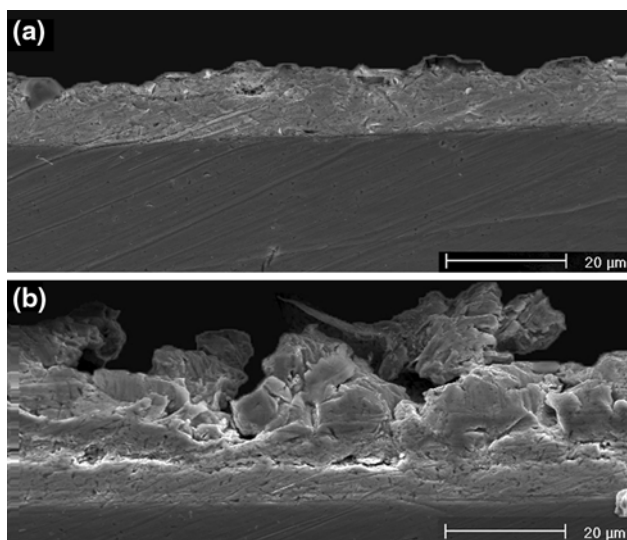


Fig. 9 Cross-sectional SEM images of LHE Cd coatings on low carbon steel shims **a** uniform cross section, **b** cross section with discontinuities

constants for the defective coatings are compared with defect-free uniform coatings as shown in Table 2. It can be observed that the uniform Zn–Ni coating provided much

better permeation resistance as compared to the coating interface with cracks and discontinuities. The microcracks are a common feature in Zn–Ni coatings, and their distribution could be due to different factors such as residual stress and also specimen geometry. The residual stresses present in the surface of the Zn–Ni coating are tensile in nature. Since the thickness of the steel substrate was 100 μm , the resistance offered by the steel substrate against bending and warping of the specimen was lower, which again resulted in non-uniform distribution of microcracks across the coating interface. Hydrogen permeation tests were also performed on Zn–Ni-coated steels that were subjected to post-plating heat treatment. From the result shown in Fig. 12, it can be observed that the breakthrough time was instantaneous and the permeation current showed an increasing trend after an initial reduction. This reduction in the permeation current following a sudden surge can be explained by the uniform monolayer close to the interface impeding further flow, which in turn resulted in an accumulation of hydrogen within the crack networks distributed randomly across the coating thickness. Once the breakthrough happened again, the flux started increasing. Because a steady state condition was not obtained and the cracked coating did not provide a uniform diffusion transient, the diffusion coefficients could not be calculated. Nevertheless, it can be observed that the permeation current was close to that of the bare steel substrate. This observation indicated that the crack network allowed the hydrogen to diffuse out when subjected to post-plating heat treatment.

The Cd coating with intermittent discontinuities also exhibited a higher permeation transient current as shown in Fig. 11b compared to the uniform coating. The discontinuities can become preferred sites for hydrogen adsorption, from where hydrogen accumulates and then permeates into the steel. A uniform coating surface would have acted as a barrier to further diffusion. This hypothesis is supported by higher subsurface hydrogen concentrations in both coatings that contained microcracks and discontinuities.

4 Discussion

From the thermal desorption studies, it was observed that a uniform, defect-free, Zn coating had the highest amount of hydrogen trapped in the interface. It was followed by the Cd coating with discontinuities in the matrix, which facilitated the escape of absorbed hydrogen.

The plating batch efficiency of Zn was 95 % since it was an acid plating solution. The plating efficiency of Zn–Ni and Cd was close to 70 % since both the processes were alkaline plating processes. Conventional understanding is that the more efficient the plating processes, the lower the

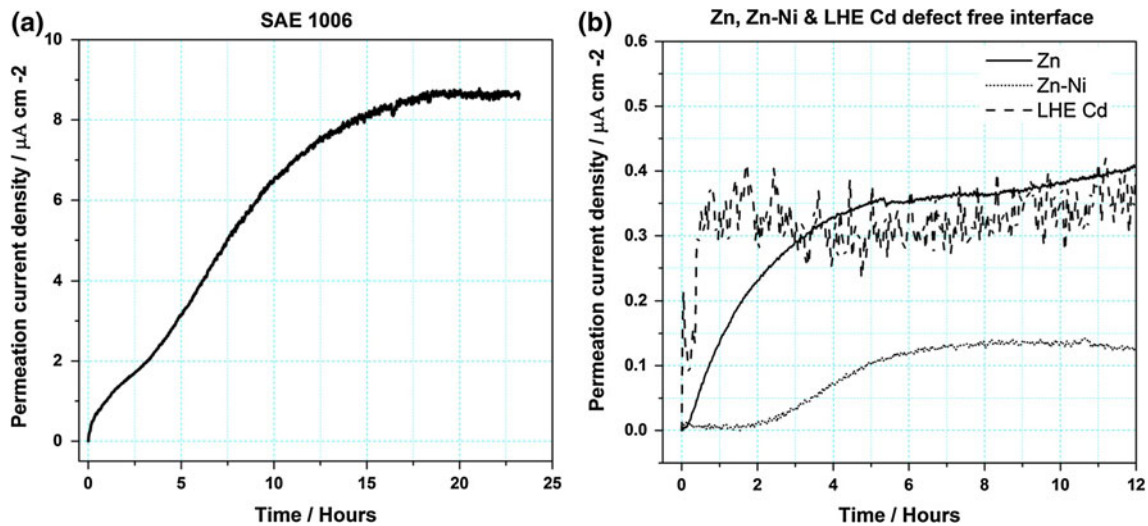


Fig. 10 H₂ permeation current density distribution with respect to time for **a** SAE 1006 steel substrate, **b** Zn, Zn–Ni, and LHE Cd coating with defect-free interface

Table 1 Diffusion coefficients and hydrogen permeability constants for steel, Zn, and Zn–Ni

Material	Diffusion coefficient $D \times 10^{-8} \text{ (cm}^2 \text{ s}^{-1}\text{)}$	Subsurface hydrogen conc. $C_0 \times 10^{-6} \text{ (Mol cm}^{-3}\text{)}$	Permeation flux $J_{ss} \times 10^{-11}$ $\text{(mol s}^{-1} \text{ cm}^{-2}\text{)}$
Bare steel	38.600	2.285	8.821
Zn	1.009	4.380	0.395
Zn–Ni	0.391	2.711	0.087
Cd	4.543	1.041	0.378

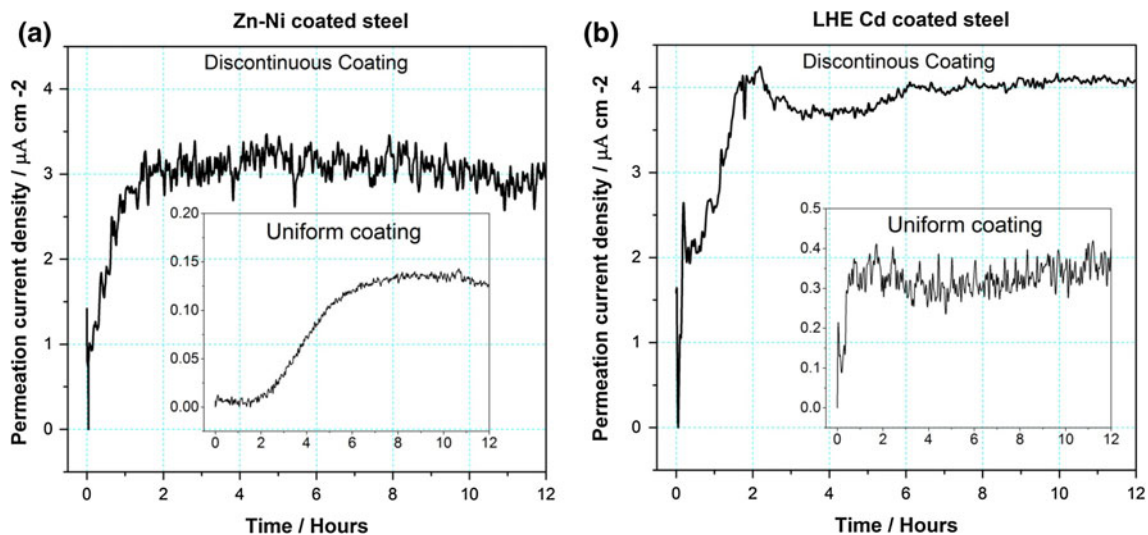


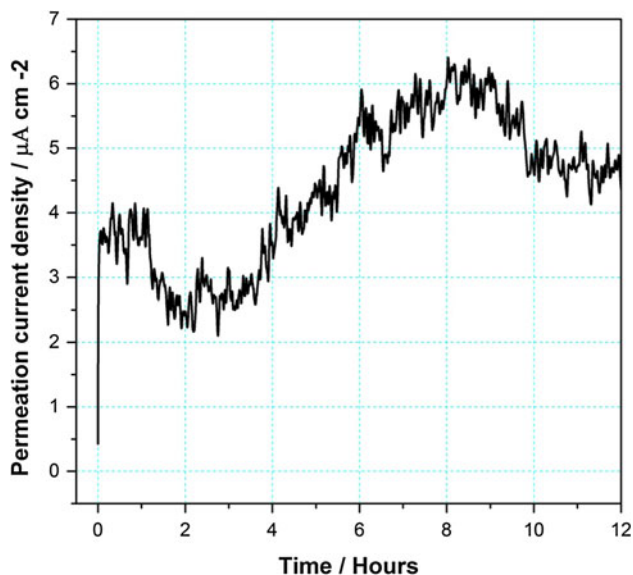
Fig. 11 Permeation current densities of **a** uniform and discontinuous Zn–Ni-coated steel, **b** uniform and discontinuous LHE Cd-coated steel

hydrogen embrittlement susceptibility. But, the thermal desorption studies in this study showed that the amount of hydrogen trapped in the Zn coating was much higher than those of the Cd and Zn–Ni coating. In the case of Zn–Ni coating, even though the bath efficiency is 70 % which

could have led to more hydrogen incorporation in the coating, the amount of hydrogen desorbed was less owing to the permeability of the coated layer. In the case of the Cd coating, since the coating contained discontinuities, these intentionally introduced discontinuities helped in

Table 2 Comparison of hydrogen permeability constants for uniform and defect-free coatings and coatings with discontinuities and microcracks

Material	Diffusion coefficient $D \times 10^{-8}$ (cm ² s ⁻¹)	Subsurface hydrogen conc. $C_0 \times 10^{-6}$ (Mol cm ⁻³)	Permeation flux $J_{ss} \times 10^{-11}$ (mol s ⁻¹ cm ⁻²)
Zn–Ni	0.391	2.711	0.087
Zn–Ni with microcracks	5.778	6.707	3.177
Cd	4.543	1.041	0.378
Cd with discontinuities	25.135	2.080	4.183

**Fig. 12** Permeation current density of Zn–Ni-coated steel subjected to post-plating heat treatment at 200 °C

hydrogen escape which is reflected from the TDS observation. The current investigation supports the hydrogen embrittlement studies evaluated by mechanical property data by Brahim and Yue [3, 27]. They observed that the bath efficiency had negligible effect compared to the current density and the plating time, since the limiting current densities would not be achieved in industrial plating processes.

The Zn–Ni coating process appears to have introduced the least amount of adsorbed hydrogen during the plating process. However, upon comparing the microstructures of the three coatings, it can be seen from Fig. 5a that Zn has a smooth uniform surface without any apparent defects or porosity. On the other hand, the Zn–Ni interface shown in Fig. 5c has microcracks which originate during plating process. These microcracks tend to increase in size if the coated part is baked, as shown in Fig. 5d. The presence of microcracks in the coating facilitates hydrogen escape, possibly reducing the hydrogen concentration in the specimen. During the baking process, as a result of development of a network of microcracks, the hydrogen diffusion was increased to a larger scale, which was evident from the permeation current observed in Fig. 12. However, the

permeability studies showed that in the absence of microcracks, (Fig. 10b) the Zn–Ni coating acted as a superior barrier against hydrogen diffusion. Conversely, in the presence of discontinuities and microcracks (Fig. 11a), hydrogen diffusion was much higher than for the uniform defect-free coating. Therefore, it is likely that the process introduced less hydrogen because the Zn–Ni coating acted as a barrier to further H absorption during the initial stages of deposition. Later, during baking, microcracks which originated due to lattice strain and mismatch facilitated the escape of any absorbed hydrogen. Combined, these phenomena led to the low quantity of hydrogen measured during the desorption test.

5 Conclusions

The Zn–Ni plating process was found to be less susceptible to IHE as compared to the Zn and Cd plating processes. The Zn–Ni plating process induced microcracks and defects in the coating microstructure. These defects expanded during the baking treatment and acted as hydrogen escape pathways. From the permeability experiments, it was observed that the defect-free Zn–Ni coating had superior resistance to hydrogen diffusion. In the presence of microcracks, the permeability of hydrogen can be improved to a large extent, which would facilitate the escape of hydrogen during post-plating heat treatment. Hence, from this investigation, it is concluded that during the initial stages of plating, the defect-free Zn–Ni layer acts as a barrier to hydrogen absorption. During the baking process, the defects present in the coating acted as a pathways for any absorbed hydrogen to diffuse out of the coated steel, thereby further minimizing the risk of embrittlement due to the plating process.

References

- Oriani RA (1978) Hydrogen embrittlement of steels. *Annu Rev Mater Sci* 8(1):327–357. doi:10.1146/annurev.ms.08.080178.001551
- Oriani RA, Hirth JP, Smialowski M (1985) Hydrogen degradation of ferrous alloys. William Andrew Publishing, Noyes

3. Brahimi S, and Yue S (2009) Effect of surface processing variables and coating characteristics on hydrogen embrittlement of steel fasteners part 2: electroplating and non electrolytic processes. In: Louisville KY (ed.) SUR/FIN, NASF, 16 June 2009
4. Coleman DH, Popov BN, White RE (1998) Hydrogen permeation inhibition by thin layer Zn–Ni alloy electrodeposition. *J Appl Electrochem* 28(9):889–894. doi:10.1023/A:1003408230951
5. Figueroa D, Robinson MJ (2008) The effects of sacrificial coatings on hydrogen embrittlement and re-embrittlement of ultra high strength steels. *Corros Sci* 50(4):1066–1079. doi:10.1016/j.corsci.2007.11.023
6. Hillier EMK, Robinson MJ (2004) Hydrogen embrittlement of high strength steel electroplated with zinc-cobalt alloys. *Corros Sci* 46(3):715–727. doi:10.1016/S0010-938x(03)00180-X
7. Hillier EMK, Robinson MJ (2006) Permeation measurements to study hydrogen uptake by steel electroplated with zinc-cobalt alloys. *Corros Sci* 48(5):1019–1035. doi:10.1016/j.corsci.2005.05.009
8. ASTM-F1941-00 (2006) F1941-00 Standard specification for electrodeposited coatings on threaded fasteners (Unified Inch Screw Threads (UN/UNR)). ASTM International, West Conshohocken, pp 19428–2959. www.astm.org. doi:10.1520/F1941-07
9. ASTM-F519-10 (2010) F519-10, Standard test method for mechanical hydrogen embrittlement evaluation of plating/coating processes and service environments. ASTM International, West Conshohocken. www.astm.org. doi:10.1520/F0519-10
10. MIL-STD-870C (2009) U.S. military standard (USAF) on cadmium plating, low embrittlement, electrodeposition. Department of defence standard practice
11. Turnbull A, Hutchings RB, Ferriss DH (1997) Modelling of thermal desorption of hydrogen from metals. *Mater Sci Eng* 238(2): 317–328. doi:10.1016/S0921-5093(97)00426-7
12. Addach H, Bercot P, Wery M, Rezzazi M (2004) Quantitative determination of hydrogen in solids by gas chromatography. *J Chromatogr A* 1057(1–2):219–223. doi:10.1016/j.chroma.2004.09.067
13. ASTM-G148-97 (2011) G148-97 Standard practice for evaluation of hydrogen uptake, permeation, and transport in metals by an electrochemical Technique. ASTM International, West Conshohocken. www.astm.org. doi:10.1520/G0148-97R11
14. Devanathan MAV, Stachurski Z (1962) The adsorption and diffusion of electrolytic hydrogen in palladium. *Proc R Soc Lond A* 270(1340):90–102. doi:10.1098/rspa.1962.0205
15. Thomas BK, Fray DJ (1981) The effect of additives on the morphology of zinc electrodeposited from a zinc-chloride electrolyte at high-current densities. *J Appl Electrochem* 11(6):677–683. doi:10.1007/bf00615170
16. Bories C, Bonino JP, Rousset A (1999) Structure and thermal stability of zinc-nickel electrodeposits. *J Appl Electrochem* 29(9):1045–1051. doi:10.1023/a:1003574625112
17. Brooks I, Erb U (2001) Hardness of electrodeposited microcrystalline and nanocrystalline gamma-phase Zn–Ni alloys. *Scripta Mater* 44(5):853–858. doi:10.1016/s1359-6462(00)0680-1
18. Bruet-Hotellaz, Bonino JP, Rousset A, Marolleau, Chauveau E (1999) Structure of zinc-nickel alloy electrodeposits. *J Mater Sci* 34(4):881–886. doi:10.1023/a:1004553803788
19. Morón LE, Méndez A, Castañeda F, Flores JG, Ortiz-Frade L, Meas Y, Trejo G (2011) Electrodeposition and corrosion behavior of Zn coatings formed using as brighteners arene additives of different structure. *Surf Coat Technol* 205(21–22):4985–4992. doi:10.1016/j.surfcoat.2011.04.090
20. Abdelhalim AM, Baghlaf AO, Sobahi MI (1984) Effect of some addition agents on the electrodeposition of cadmium from acidic chloride baths. *Surf Technol* 22(2):129–142. doi:10.1016/0376-4583(84)90049-9
21. Elhalim AMA, Sobahi MI (1983) Effect of bath constituents and some plating variables on the electrodeposition of cadmium from acidic chloride baths. *Surf Technol* 19(1):45–57. doi:10.1016/0376-4583(83)90018-3
22. Lin C, Lee H, Hsieh S (1999) Microcracking of flash coatings and its effect on the Zn–Ni coating adhesion of electrodeposited sheet steel. *Metall Mater Trans A* 30(2):437–448. doi:10.1007/s11661-999-0333-0
23. Sasaki T, Hirose Y (1994) Residual stress distribution in electroplated Zn–Ni alloy layer determined by X-ray diffraction. *Thin Solid Films* 253(1–2):356–361. doi:10.1016/0040-6090(94)90347-6
24. Boes N, Züchner H (1976) Electrochemical methods for studying diffusion, permeation and solubility of hydrogen in metals. *J Less Common Metals* 49:223–240. doi:10.1016/0022-5088(76)90037-0
25. Cao Y (2002) Influence of structure of palladium and nickel based membranes on hydrogen permeation. Thesis (Ph D), McGill University, Montreal, Quebec, Canada
26. Early JG (1978) Hydrogen diffusion in palladium by galvanostatic charging. *Acta Metall* 26(8):1215–1223. doi:10.1016/0001-6160(78)90005-6
27. Brahimi S (2007) Effect of surface processing variables on hydrogen embrittlement of steel fasteners. Thesis (M Eng), McGill University, Montreal, Quebec, Canada